Snell or Fresnel – The influence of material index on hyper NA lithography

Bruce Smith and Jianming Zhou
Rochester Institute of Technology, Center for Nanolithography Research
Microelectronic Engineering Department, 82 Lomb Memorial Dr., Rochester, NY 14623

ABSTRACT

As immersion lithography is extended to ever increasing resolution, the resulting propagation angles in the materials involved become closer to grazing than to normal incidence. Classical laws of refraction and reflection cannot be used with either assumption however, as a collection of angles may exist across the entire range. Fresnel reflection at these angles becomes large enough that small disparities in refractive indices at material interfaces may lead to adverse effects. As an example, when water is used at numerical apertures approaching its refractive index, reflection effects are greater than the constraints imposed by refraction or absorption. This will limit the maximum NA value allowed by any given material to values sufficiently lower than its refractive index. Additionally, we have grown accustom to expanding the application of the Snell-Descartes Law to materials with low absorption, assuming that the contribution of the imaginary component of the refractive index is negligible. This is not the case for photoresists, fluids, or glasses, which can not strictly be considered as non-absorbing media. We have expanded the Snell-Descartes Law for absorbing media, with some interesting consequences. We will show that there is no real limit on the numerical aperture into a material, so long as its extinction coefficient is not zero. The relationship that lithographers have been using recently where NA< $\min[n_{glass}, n_{fluid}, n_{resist}]$ will be shown to be inadequate and imaging at numerical apertures up to 1.85 will be demonstrated using materials with significantly lower (real) refractive index values.

Keyword list: Hyper-NA, reflection, refraction, Snell's Law, Fresnel, immersion lithography

1. INTRODUCTION

Several challenges exist as immersion lithography is employed for hyper-NA lithography, where angles into the media involved are becoming oblique. The angles in the media as well as at media interfaces become large and both reflection and refraction effects need to be more carefully understood. Assumptions that lithographers have been made in the past of "near normal incidence" are no longer valid as "near grazing incidence" is approached. As an example, the 90nm half-pitch generation results in angles of 26° in a photoresist (with an real refractive index of 1.71) verses an angle of 45° for 45nm half-pitch geometry. There are also strong differences in polarization states for both reflection and interference for the later case.

Figure 1 shows recent images obtained using oblique angle interferometic lithography at a 193nm wavelength using either fused silica (amorphous SiO_2) or sapphire (crystalline Al_2O_3) optical elements. Each SEM image is representative of the resolution that has been obtained at a given numerical aperture using these elements, imaging into a photoresist with a refractive index of 1.71. Superimposed on each image is the ray angles that are propagated into each media involved with the imaging, where PR represents the photoresist material and the fluid in all cases is water (with a real refractive index of 1.44 at 193nm). As angles approach critical, total internal reflection (TIR) results and imaging is made possible by propagating the evanescent field in the thin media to underlying layers [1]. As the numerical aperture of the system increases, the angle in the fluid approaches and exceeds TIR, as do the angles in the photoresist. At 1.85NA, the angle in the sapphire optics is 74°. The questions come down to how difficult such imaging would be for the manufacture of devices and whether this is driven more by refraction or reflection.

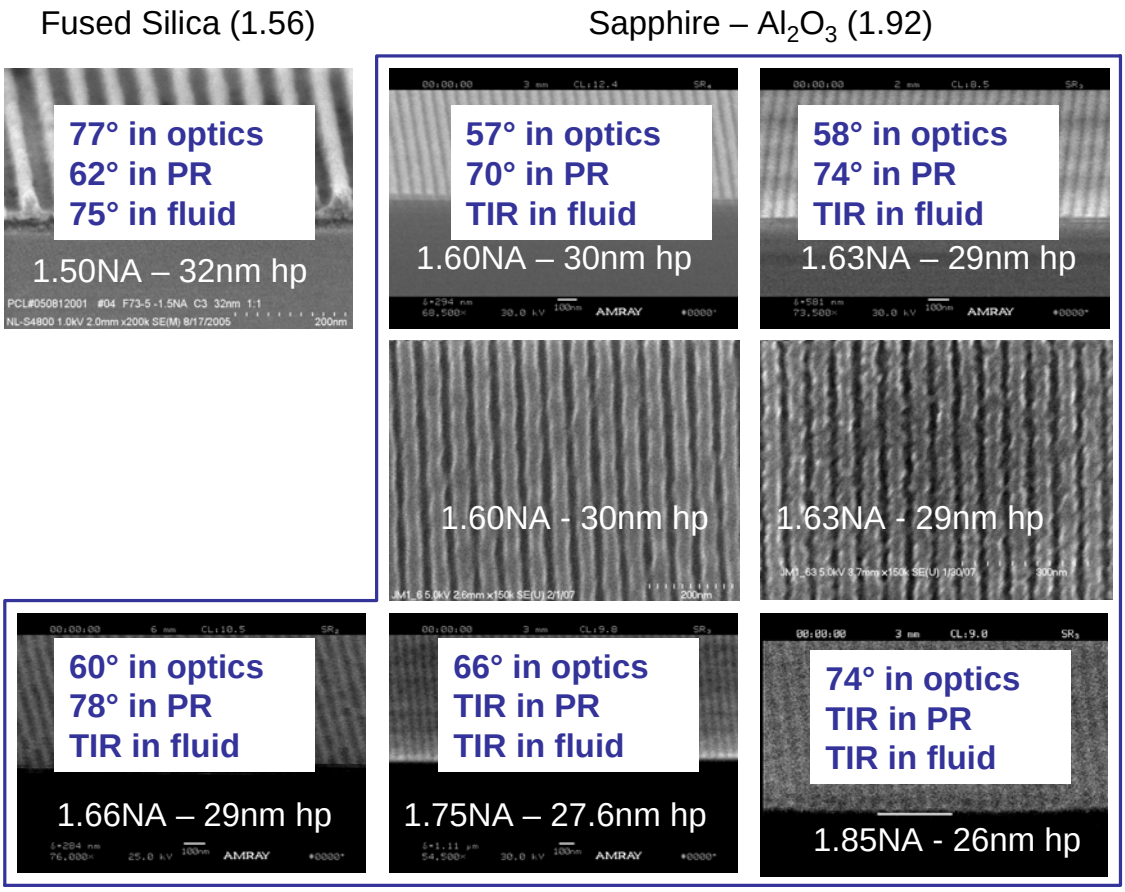

Figure 1. SEM images of 193nm interferometric imaging using fused silica (top-left) and sapphire optical elements, showing the refracted angle into corresponding media.

2. THE ROLE OF FRESNEL REFLECTION IN HYPER-NA LITHOGRAPHY

The Fresnel reflection coefficients are the key to the description of the propagation of radiation through stratified media. The coefficients, and the corresponding reflectance relationships, were derived by Augustin Fresnel in 1866 prior to Maxwell's electromagnetic theory band provide a complete description of the phenomena [2]. The basic equations are well documented, where the reflection (R) for TE and TM reflection is calculated as:

$$R_{TE} = \left[\frac{n_1 \cos(\theta_i) - n_2 \cos(\theta_t)}{n_1 \cos(\theta_i) + n_2 \cos(\theta_t)} \right]^2 \qquad R_{TM} = \left[\frac{n_1 \cos(\theta_t) - n_2 \cos(\theta_i)}{n_1 \cos(\theta_t) + n_2 \cos(\theta_i)} \right]^2$$

At normal incidence, the dependency on polarization is removed and Fresnel reflection simplifies to:

$$R = R_{TE} = R_{TM} = \left[\frac{n_1 - n_2}{n_1 + n_2} \right]^2$$

The plot in Figure 2 shows the reflectance for TE and TM polarization for an arbitrary thin film combination, showing both the increase in reflectance and the increase in the disparities of polarization states as the angle at the interface increases. The Brewster angle (where the electric field lies in the same plane as the incident ray and the surface normal) and the Critical angle (where angle beyond this results in total internal reflection) are labeled. As with many things involved with the fabrication of semiconductor integrated circuits (ICs), a timeline can be placed on such a plot to emphasize the changes occurring in the technology. Whereas prior to 2001, incident angles were small and near-normal incidence could be assumed, angles today are no longer small and the near future brings angles that are approaching oblique.

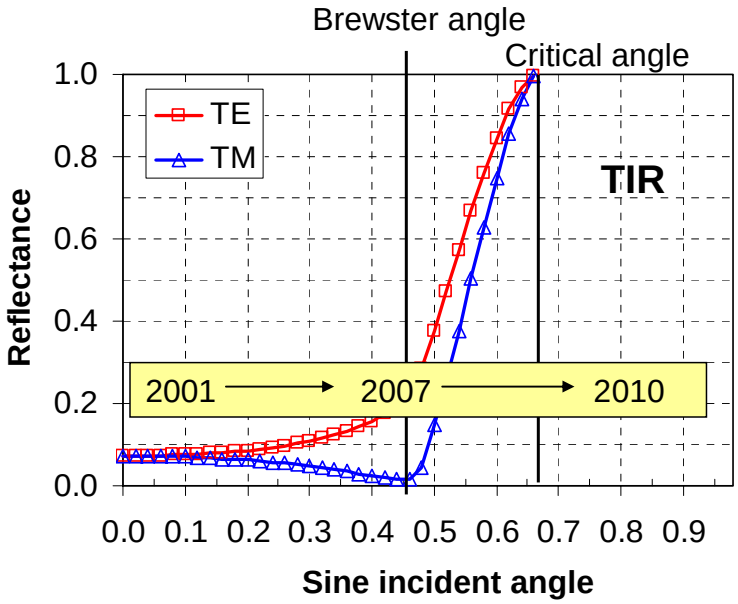

Figure 2. A reflection plot for increasing angles, demonstrating the increasing angles with past and future lithography generations.

2.1 Reflection at a water-optics interface

The first situation that we consider is the reflectance at the interface between the last optical lens element and water as an immersion fluid. Four optical element materials are considered: fused silica, barium lithium fluoride ($BaLiF_3$) sapphire (crystalline Al_2O_3), and lutetium aluminum garnet (LuAG). The later three materials are attractive alternatives to fused silica as they posses high transmission with relatively large refractive index values (1.65, 1.92, and 2.14 respectively). The reflection at interfaces is equivalent regardless which media (fluid or optic) is incident and the results are shown in Figure 3. The TE reflectance is larger than that for TM; both which can be summarized for various element types for 1.30NA imaging (for 64° or $\sin\theta = 0.9$ in the water fluid) as:

$R_{TE}(0.9)$ at interfaces:
- Fused silica (1.56) – 4%
- $BaLiF_3$ (1.64) – 6%
- Sapphire (1.92) – 14%
- LuAG (2.14) – 20%

$R_{TM}(0.9)$ at interfaces:
- Fused silica – <1%
- $BaLiF_3$ – 2%
- Sapphire – 3%
- LuAG – 3%

It is interesting to note that although the reflectance at the water and fused silica interface at normal incidence is very low (and considered a benefit over air-imaging in early evaluation of the merits of immersion lithography), the reflectance at this angle is as large as that for normal incidence in air. Although the reflectance is extreme for LuAG with water, this is not such a concern since it is likely that a higher refractive index fluid would be employed for use with this material. In all cases, the disparity between TE and TM polarization states is large and would need to be addressed through the use of a thin film optical coating at the interface. Such thin film materials would need to possess high transmission and durability (radiation and chemical), with compatibility to both the optical and fluid media surrounding

it. The choice of high refractive index thin film materials for this application may be limited and solutions may be more difficult is a multilayer design was required.

2.2 Reflection at high index fluid – optics interface

The second situation considered is the reflectance resulting for a high index fluid (HIF) with a refractive index of 1.65 used as an immersion media in contact with a final element material. Since there is a near index match with $BaLiF_3$, the resulting reflection is low. Figure 4 is a plot of the reflectance at the fluid interface for fused silica and LuAG for TE and TM polarization. The reflectance for fused silica is below 6% for TE polarization (and 3% for TM polarization) but it is high for LuAG, at over 12% and 1.5% for TE and TM respectively. This situation may present difficulties with imaging without methods of reflection control. It is expected that the contribution of this amount of reflectance to flare would be significant, which would increase at larger angles. It should also be noted that the reflectance (and resulting flare) is dependant on angle, and thus would increase also with the larger diffraction angles of smaller geometry. More rigorous analysis of the contribution of this effect to image degradation is necessary to understand its full impact.

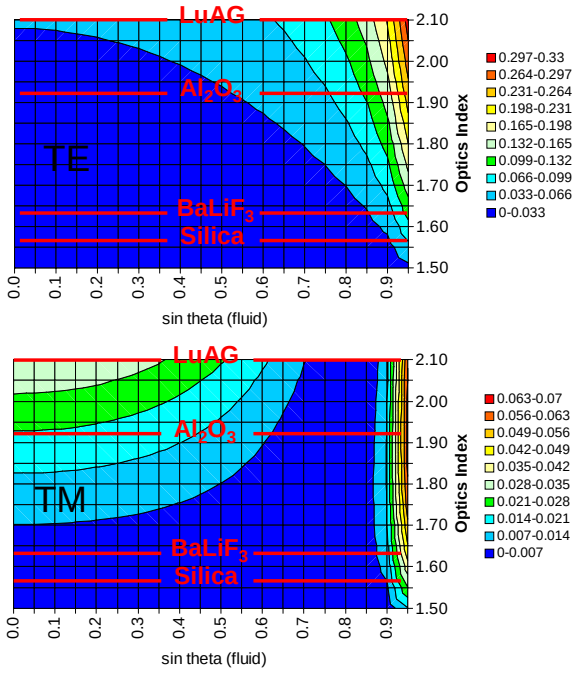

Figure 3. The reflectance at the interface between water and final optical element materials for 193nm immersion lithography at 1.30NA.

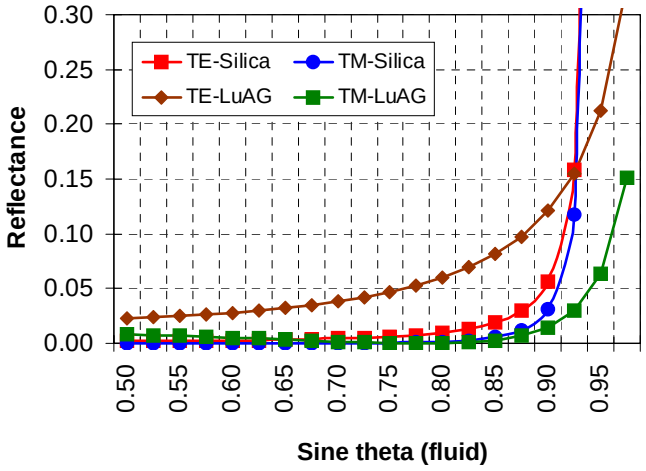

Figure 4. The reflectance at the interface between a high index fluid (n=1.65) and final optical element materials for 193nm immersion lithography at 1.50NA.

A summary of the TE and TM reflectance for 1.50NA imaging (for 64° or sinθ=0.9 in the high index fluid) with fused silica and LuAG is below:

$R_{TE}(0.9)$ at interfaces:
Fused silica (1.56) – 5.6%
LuAG (2.14) – 12%

$R_{TM}(0.9)$ at interfaces:
Fused silica (1.56) – 5.6%
LuAG (2.14) – 12%

2.3 Reflection at the resist-fluid interface

Next, we consider the reflection at the bottom of the fluid, at the interface with the photoresist stack, as shown in Figure 5.

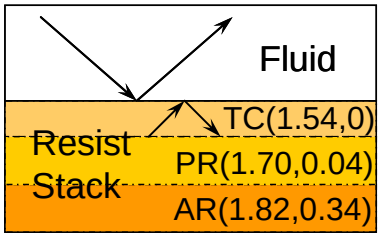

Figure 5. A depiction of the reflectance at the interface between an immersion fluid and a photoresist stack, which includes a top-coat (TC), photoresist (PR), and anti-reflection bottom coating (AR).

In this case, the bottom AR coating is chosen as an infinite media and the photoresist layer is fixed at a thickness of 80nm. Plots in Figure 6 show the TE and TM reflectance as a top-coat (TC) layer is varied from 0nm to 65nm. With no TC film, the reflectance at normal incidence is low for angles in the fluid up to 30°. Since this example uses water as the imaging media, this corresponds to a numerical aperture of just 0.72. As angles are increased, the reflectance increases rapidly. This can be reduced through the use of a TC layer, which acts as an AR as angles for path lengths through the layer corresponding to quarter wave film thicknesses. This can be seen as the TC film thickness is increased, where the reflectance minima progresses to larger angles. The problem seen here is that this reduction at larger angles is at the cost of increased reflectance at smaller angles, where a 65nm TC film reduces reflectance to less than 1% at 65° (1.30NA) but increases it to nearly 9% at 48° (1.07NA). Since the photoresist stack itself is a stratified media, it would be logical to attempt to optimize the entire system to reduce the fluid-resist reflectance. The potential for success is limited, where the reflectance can be brought to values below 1% but little improvement across a range of angles is achieved. The situation is further complicated when we consider that the photoresist reflectivity control at both its front-side and back-side. This represents a classical thin films scenario, where the photoresist would be considered the “substrate” and the TC and bottom AR layers are used to control the reflectance at both surfaces. Various efforts are underway to use multilayers on the back-side of the photoresist to reduce reflectivity [3],[4]. Though the use of photoresist without top-coat layers may be desirable from a processing standpoint [5], it will be difficult to achieve adequate reflection control without at least a single layer film. The ideal direction to reduce or eliminate these reflection effects would be toward a multi-layer TC, which would present an additional set of challenges from an integration standpoint.

2.4 Reflectance at the substrate-resist interface

The control of the reflectance below the photoresist has been one that has been studied and optimized for many lithography generations, though the use of single-layer or more recently multi-layer bottom AR coatings (BARCs). The situation for hyper-NA imaging requires more careful consideration not only of the residual reflection remaining after the implementation of a BARC, but also the position of the standing wave node in the very thin resist films that are being emplyed. As an example, the plot in Figure 8 shows how the constructive standing wave node present in a resist film with very low levels of reflectance (near 1%) dramatically influence the photoresist profile. This is a situation using a single layer BARC for use at just one interference angle for imaging, specifically 1.05NA for 45nm half-pitch imaging. The photoresist layer thickness is 80nm and the BARC material has a complex refractive index of (1.82, 0.34). Plots show the reflectance curves along with simulated profiles (ILSim) and experimental results. The selection of first minima or higher harmonics will be determined by the desired resist profile, especially at the resist-substrate interface.

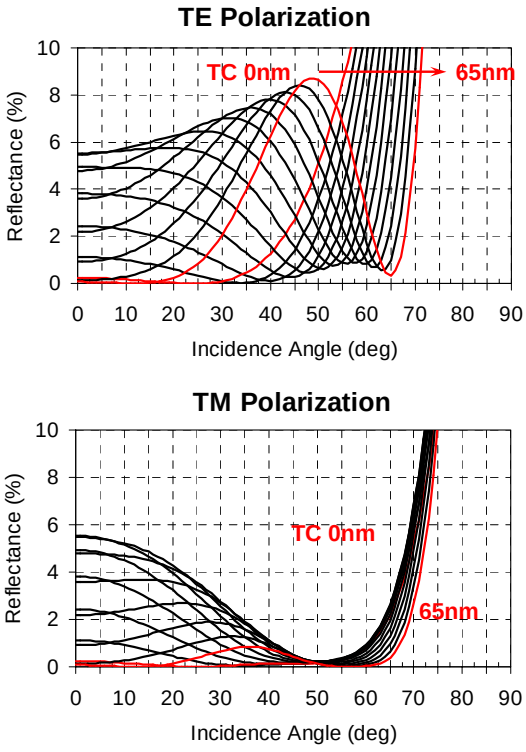

Figure 6. The variation of reflectance at the fluid (water) photoresist (PR) stack interface with increasing TC film thickness for TE and TM polarization, using the stack parameters in Figure 5.

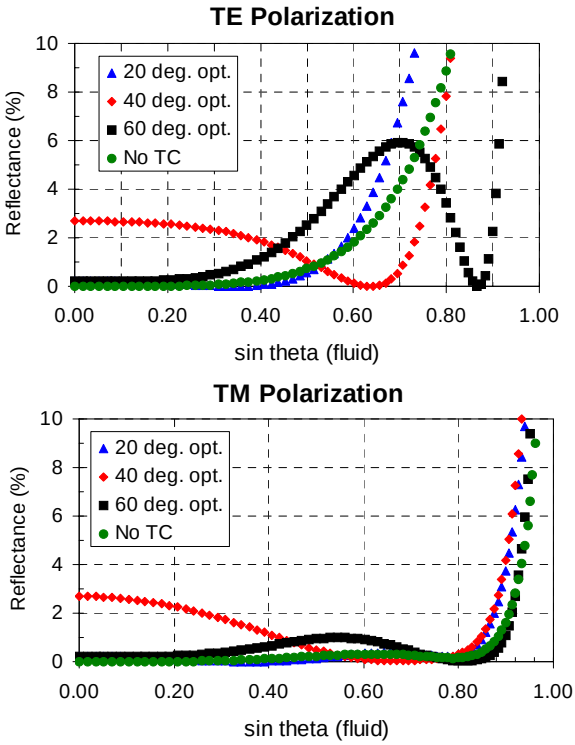

Figure 7. The variation of reflectance at the fluid (water) photoresist (PR) stack interface with optimization of TC and photoresist parameters, where the layers for 20° optimization are 50nmTC/40nmPR, the layers for 40° optimization are 60nmTC/44nmPR, and the layers for 60° optimization are 72nmTC/65nmPR.

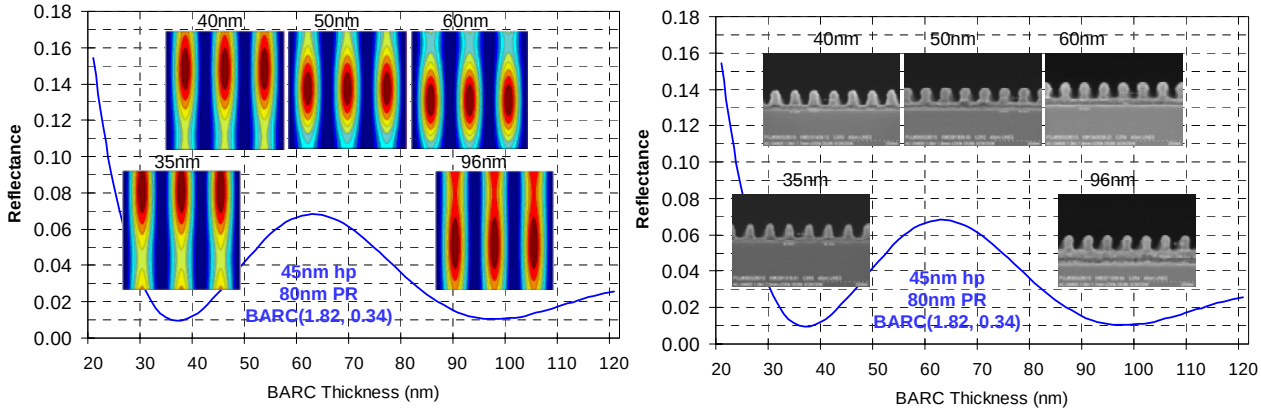

Figure 8. Reflectance curves for the optimization of a single layer BARC at 1.05NA, showing simulated standing wave profiles (left) and experimental results (right) for 1st minima and 2nd minima locations, where the constructive standing wave node position in the resist layer is influenced by BARC thickness.

2.5 Four beam interference at the substrate-resist interface.

The root cause for resist standing waves is identical to that which is responsible for imaging, namely interference. As we approach angles of 45° in photoresist (which corresponds to a numerical aperture of 1.20), these two phenomena can become identical. As an illustration, Figure 9 shows how the contribution of two-beam interference and two-beam reflectance can interact to produce more or less pronunciation of a standing wave pattern imaged to the scale of a desired interference image pattern. If reflection is maximized rather than minimized, a four-beam interference situation can result, where the standing wave is as pronounced as the patterned image. The result could be the construction of "nanochannels" images laterally into the photoresist film. Though this condition may be interesting enough, the condition presented with TM polarization becomes more intriguing, as we consider how interference in this polarization state will go though a change of phase at an interfering angle of 90°. Figure 10 is a simulation of standing wave intensity patterns in a photoresist film at varying angles, illuminated with TE and with TM polarization (simulations carried out using Prolith v.9). As the angle is increased, the nodal spacing in the photoresist film increases as expected with 1/cos(θ), regardless of polarization. The TM state of polarization , however, goes through a phase change at 45° (or sin(θ) = 0.707), where near-constructive interference in the transitional image region at the resist-substrate interface is no longer in phase with the TE case. This phenomena can have interesting effects on the four beam interference by maximizing reflection at the boundary, as seen in Figure 11 in the intensity profiles in resist over silicon for numerical aperture values between 0.54 and 1.38 (simulations carried out using ILSim). Figure 12 shows an ideal scenario for TM polarization, where contrast in the standing wave anti-node at diagonal locations is as large as that for the nodes, resulting in a frequency doubling of the nanochannels in the resist film. In this example, 40nm channels are imaged into the resist film with an aspect ratio of 1.0. Nanospheres could be imaged from the interference of four-beams, resulting in a total of eight beams upon reflectance. Applications in nanophotonic crystals or the nanotechnology fields may result.

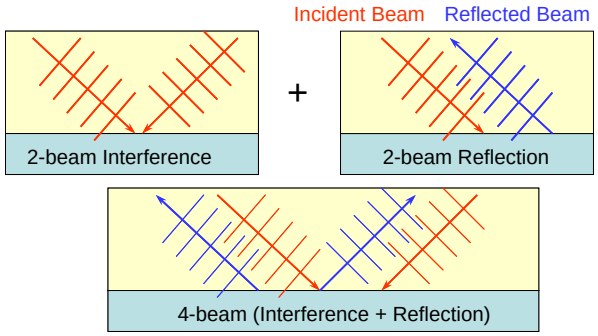

Figure 9. Four-beam imaging resulting from the combination two-beam incident interference and two-beam reflectance interference.

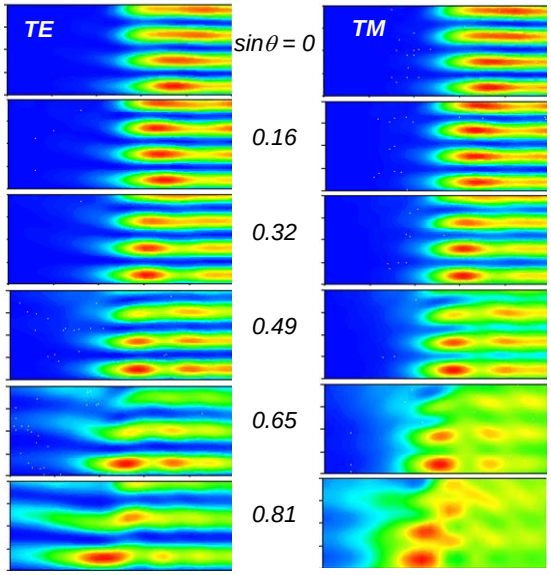

Figure 10. (Above). The standing wave intensity in a photoresist film for TE and TM polarization for varying angles in the photoresist.

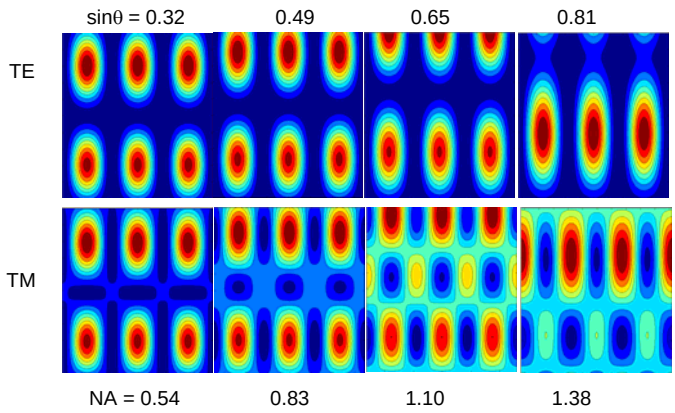

Figure 11. (Left). Intensity profiles in resist over silicon for varying angles from the combination two-beam incident interference and two-beam reflectance interference for TE and TM polarization.

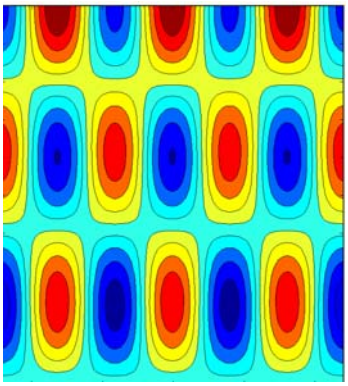

Figure 12. Nanochannel imaging of 40nm channels using TM polarization at 1.20 NA in resist over silicon.

3. SNELL-DESCARTES LAW OF REFRACTION AND ABSORBING MEDIA

In our previous paper [1], we reported on the imaging of 26nm half-pitch geometry at a numerical aperture of 1.85 into a photoresist with a real refractive index of 1.71. Though this appeared to go against conventional wisdom that the propagation of energy into the photoresist would not be possible if the resist media refractive indexwas not at least as large as the imaging numerical aperture, this reasoning fails to account for refractive effects from absorption. There may be contribution to this imaging from scatter effects from small PAG particles in the resist, or possible photon capture mechanisms by the small particles during sufficient photon dwell time, but the dominant reason for such imaging is absorption.

Several attempts have been made to extend the Snell-Descartes law of refraction for absorbing media [6], [7]. Problems arise with treatments that lead to incomplete descriptions for the contribution of polarization to refraction, which suggest an influence from absorption for TM polarization and none for TE polarization. The simple substitution of the complex refractive index ($n^*=n-ik$) into the Snell-Descartes law does lead to a solution, albeit one with a complex angle with little physical meaning for reconciliation. Instead, an approach that combines expressions for planes of equal phase and magnitude is required, which is described in more detail in our companion paper [8]. By defining an effective refractive index, n', which is defined by incident (media 1) and transmitted (media 2) angles as:

$$\frac{\sin\theta_1}{\sin\theta_2} = n'$$

the effective refractive index for media 2 becomes:

$$n' = \left\{ \frac{n^2 - k^2 + \sin^2\theta_1 \pm \sqrt{\left(n^2 - k^2 + \sin^2\theta_1\right)^2 - 4\left[\left(n^2 - k^2\right)\sin^2\theta_1 - n^2k^2\right]}}{2} \right\}^{\frac{1}{2}}$$

where n and k are normalized to the first media. The effective refractive index is dependent on the angle into the media as well and the real and imaginary refractive indices of the transmitting media. The effective extinction coefficient scales with the effective refractive index as:

$$k' = \frac{nk}{n'}$$

Figure 13 shows the plot of the effective refractive index as the numerical aperture into the media 2 (n_2'sinθ) verses the product of the real refractive index and sinθ, which would be equivalent to NA for non-absorbing media. The conditions plotted are for photoresist as media 1 and sapphire as media 2, where the maximum numerical aperture allowed is 1.92, limited by the index of the sapphire. For an extinction coefficient (k) greater than zero, it becomes

apparent that any numerical aperture can be captured in a photoresist film, where the departure from linearity increases with absorption. Imaging results using three numerical apertures (1.66, 1.75, and 1.85) are indicated on the plot as well, leading to an explanation for the seemingly anomalous results. It would be anticipated that if the increase in system numerical aperture were continued, failure would not be attributed to the loss of propagating refraction.

Though this result seems be exploitable by lithographers, it should be realized that even small values for the resist extinction coefficient at such large angles will lead to significant absorption, since the increases follow with a 1/cosθ trend. Figure 14 shows how the effective absorption at angles corresponding to numerical apertures between 1.0 and 1.7 increases dramatically. Two imaging results are indicated on this plot, for 1.75NA and 1.85NA, where it is seen that the increase in absorption for the 1.85NA case is more than 30X that which would be anticipated for higher refractive index resist materials. This result is confirmed in the exposure times required for this condition, as well as the shallow depth of the image in the resist film. This plot suggests that a resist refractive index approaching 1.90 would be desirable for numerical apertures of 1.70. A numerical aperture of 1.60 could benefit from in increase in refractive index to near 1.78.

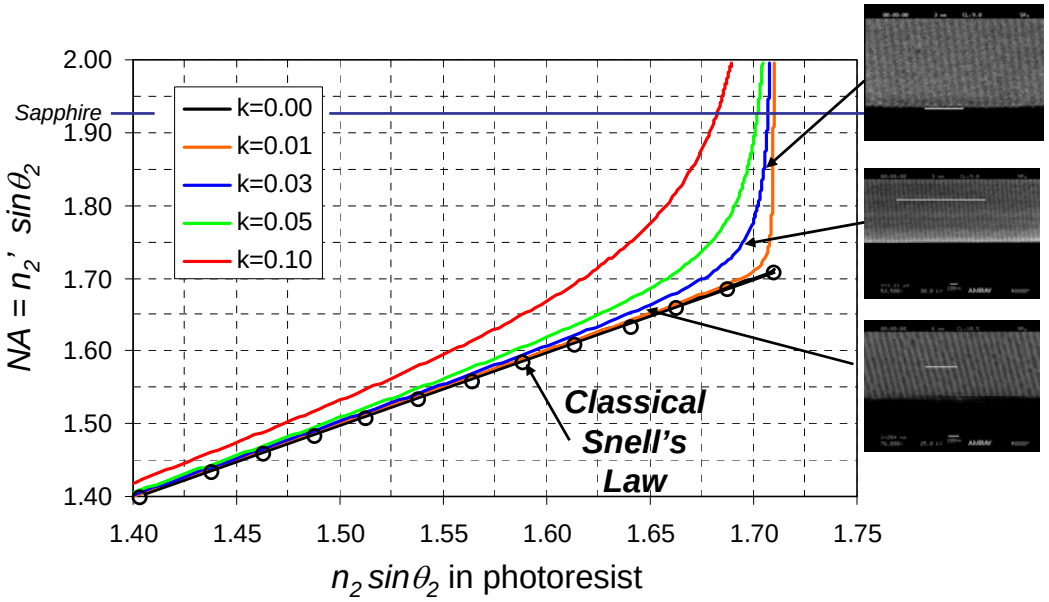

Figure 13. A plot of the influence of extinction coefficient on the refraction of radiation from sapphire (1.92) into photoresist (1.71), for values from 0.0 to 0.10.

4. CONCLUSIONS

The Fresnel reflection at interfaces in lithography media is becomingly increasingly important as incidence angles are increased. Assumptions of near-normal incidence are no longer valid and each interface needs to be evaluated uniquely. Polarization effects will dominate at these large angles and additional thin film coating may need to be employed to reduce them. The use of stratified thin films for the reduction of reflection has been utilized for nearly two centuries and is well understood. Such technologies will need to be employed at optics/fluid and fluid/resist stack interfaces to achieve reflection at levels below a few percent. This may present compatability, durability, and material selection problems for optical coatings in contact with immersion fluids. A more difficult problem may be the suggestion that a resist may require a multilayer top-coat for the reduction of reflection.

It is not surprising that errors would exist with the extrapolation of refractive laws to large angles if absorbing media were assumed to be non-absorbing. Nanolithography presents the first real opportunity to appreciate this error, as we are now imaging at oblique angles and at depths equivalent to a fraction of a wavelength. Additionally, though

absorption exists, it is still weak, allowing image capture which otherwise is impossible in strongly absorbing media. By including the contribution of absorption to refraction effects, it is seen that both material properties need to be considered together as the limits of photoresist imaging are considered or as new materials are explored.

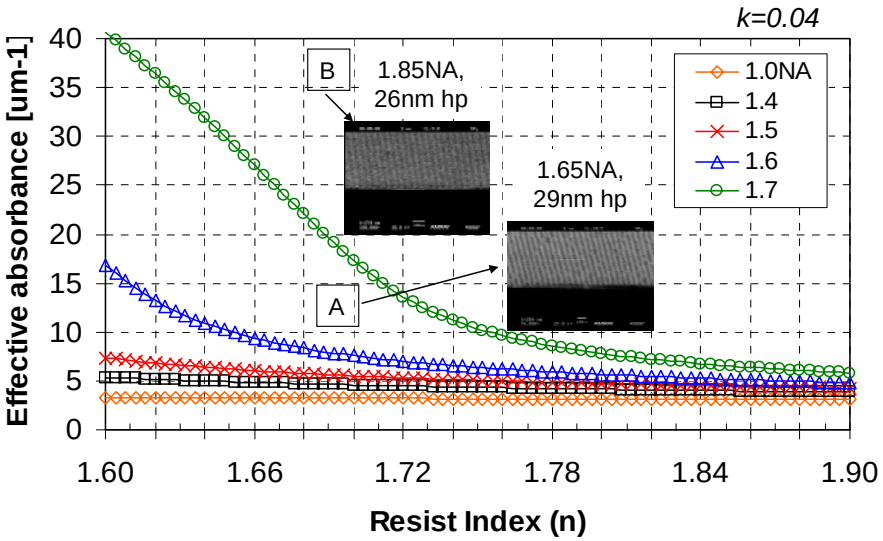

Figure 14. The effective absorbance for an extinction coefficient of 0.04 with varying resist refractive index and imaging numerical aperture.

ACKNOWLEDGEMENTS

The authors wish to acknowledge Intel and the Semiconductor Research Corporation for support and KLA-Tencor for the use of Prolith simulation software.

REFERENCES

[1] B.W. Smith, Y. Fan, J. Zhou, N. Lafferty, A. Estroff , "Evanescent wave imaging in optical lithography," Proc. SPIE Optical Microlithography XIX, **6154**, 2006.
[2] A. Fresnel, "Memoire sur la loi des modifications que la reflection imprime a la lumiere polaisee," in Ouvres Completes de Fresnel, **1**, 767-775, 1866.
[3] B.W. Smith, L. Zavyalova, A. Estroff, "Benefiting from polarization - effects of high-NA on imaging," Proc. SPIE **5377**, 2004.
[4] D. J. Abdallah, M. Neisser, R. R. Dammel, G. Pawlowski, S. Ding, F. M. Houlihan, A. R.Romano, "193nm dual layer organic BARCs for high NA immersion lithography," Proc. SPIE **5753**, 417-425, 2005.
[5] Y Wei, N. Stepanenko, M Sebald, "Evaluation of 193-nm immersion resist without topcoat," J. Microlith., Microfab., Microsyst., **5(3)** , 0330021-8, 2006.
[6] T.A. Kudykina, "Boundary conditions in case of electromagnetic wave absorption," Phys. Stat. Sol. (b), **106**(1), 365-373, 1990.
[7] A.V. Sokolov, "Optical properties of metals," GIFML, Moscow, 1961.
[8] J. Zhou, N. Lafferty, A. Bourov, B.W. Smith, "Immersion lithography with numerical apertures above 2.0 using high index optical materials," Proc. SPIE Optical Microlithography XX, **6520**, 2007.